REVISTA ELETRÔNICA CIENTÍFICA DA UERGS

Sodium tetratungstate/tungsten oxide films prepared with dodecyltrimethylammonium chloride as structuring agent

Diego Soares de Moura
Universidade Federal do Rio Grande do Sul (UFRGS).
E-mail: diegosdemoura@gmail.com, http://lattes.cnpq.br/3742601224153239

Irene Teresinha Santos Garcia
Universidade Federal do Rio Grande do Sul (UFRGS).
E-mail: irene.garcia@ufrgs.br, http://lattes.cnpq.br/2296402907146130

ISSN 2448-0479. Submetido em: 01 ago. 2022. Aceito: 18 nov. 2022.
DOI: http://dx.doi.org/10.21674/2448-0479.83.218-227

Abstract
The multiple forms of structuring transition metal anions in solution are important aspects to be taken into account in obtaining oxides of these metals by the sol-gel method. The formation of polyanions in aqueous media can produce a variety of structures in the solid state. Films were obtained through sol-gel method with sodium tungstate as precursor and dodecyltrimethylammonium chloride (DTAC) as structuring agent, after calcined at 700 °C in air. The films, structured as nanospheres, were composed mainly of triclinic sodium tetratungstate and monoclinic tungsten oxide. The cationic surfactant interacts in aqueous media with the precursor, affecting the obtained films' final morphology, without affecting their crystal structure. Their photocatalytic properties were also evaluated.

Keywords: Colloidal synthesis; sol-gel; photocatalysis.

Resumo
Filmes de tetratungstato de sódio/óxido de tungstênio preparados com cloreto de dodeciltrimetilamônio como agente estruturante
As múltiplas formas de estruturação de ânions de metais de transição em solução revelam aspectos importantes a ser levados em consideração na obtenção de seus óxidos pelo método sol-gel. Um desses aspectos é a formação de poliânions em meio aquoso, que pode produzir uma variedade de estruturas no estado sólido. Desta feita, foram obtidos filmes através do método sol-gel utilizando-se, como precursor, de tungstato de sódio e, como agente estruturante, cloreto de dodeciltrimetil amônio, que foram posteriormente calcinados a 700 °C em ar. Observou-se que os filmes, estruturados como nanoesferas, eram compostos principalmente de tetratungstato de sódio triclínico e óxido de tungstênio monoclínico. Por sua vez, conclui-se que o surfactante catiônico interage em meio aquoso com o precursor e afeta a morfologia final dos filmes obtidos, no entanto tem pouca influência nas suas estruturas cristalinas. Faz-se importante destacar que as propriedades fotocatalíticas foram também avaliadas na presente pesquisa.

Palavras-chave: Síntese coloidal; sol-gel; fotocatálise.

Resumen
Películas de tetratungstato de sodio/óxido de tungsteno preparadas con cloruro de dodeciltrimetilamonio como agente estructurante
Las múltiples formas de estructurar los aniones de metales de transición en solución son aspectos importantes a tener en cuenta a la hora de obtener sus óxidos por el método sol-gel. La formación de polianiones en

medios acuosos puede producir una variedad de estructuras en estado sólido. Se produjeron películas por medio del método sol-gel utilizando tungstato de sodio como precursor y cloruro de dodeciltrimetilamonio como agente estructurante, luego calcinadas a 700 °C en aire. Las películas, estructuradas como nanoesferas, estaban compuestas principalmente de tetratungstato de sodio triclínico y óxido de tungsteno monoclínico. El tensioactivo catiónico interactúa en medio acuoso con el precursor, afectando la morfología final de las películas obtenidas, pero tiene poca influencia sobre su estructura cristalina. Fueron evaluadas también las propiedades fotocatalíticas.

Palabras clave: Síntesis coloidal; sol-gel; fotocatálisis.

Introduction

Tungsten oxides are semiconductor materials that have been widely studied due to their photochromic (ZHANG *et al.*, 2021) and electrochromic (KUMAR *et al.*, 2022) properties. As supported films, their use as smart windows, gas sensors and photocatalysts (PURUSHOTHAMAN; MURALIDHARAN; VIJAYAKUMAR, 2021; CORRÊA *et al.*, 2014) can be highlighted. These oxides can be prepared as powder or thin nanostructured films (MARINHO, J. Z; PATROCINIO, A. O. T., 2022). These oxides present several stoichiometries, crystal structures and morphologies and can be synthetized by different processes such anodization (DA COSTA *et al.*, 2021; DA COSTA *et al.*, 2015), electrodeposition (GURCUOGLU; EVECAN; ZAYIM, 2015), chemical vapor deposition (NAVIO *et al.*, 2012), physical vapor deposition (GARCIA *et al.*, 2015), hydrothermal (YANG *et al.*, 2012) and sol-gel (DE MOURA *et al.*, 2018; PAZINATO *et al.*, 2019) methods.

The sol-gel process allows different structuring modes and consists in the conversion of a stable colloidal dispersion (sol) into a three-dimensional network (gel) (SANTATO *et al.*, 2001). The traditional method consists of reacting an oxide precursor, dispersed or dissolved in liquid media, at low temperatures and is classified as aqueous or non-aqueous (PICQUART *et al.*, 2000). Precursors such as sodium tungstate, tungstic acids or tungsten are widely used in aqueous media (TAHIR *et al.*, 2017), while tungsten chloride is used in alcoholic medium (WANG; CHOU; LIU, 2003). The aqueous sol-gel process using sodium tungstate is environmentally friendly and low-cost, being widely used in tungsten oxide synthesis.

When sodium tungstate is used as precursor, its conversion to tungstic acid is obtained by addition of hydrochloric acid (TAHIR *et al.*, 2017). However, the use of sodium tungstate as precursor can affect the purity of the tungsten oxide. During the calcination process, sodium tungstate not converted to tungstic acid reacts with tungsten oxide producing a mixture of polytungstates, mainly $Na_2W_2O_7$ and $Na_2W_4O_{13}$ (SCHOFIELD, 2003). The band gap of $Na_2W_4O_{13}$ (VAMVASAKIS *et al.*, 2015; SHAMAILA *et al.*, 2011) is 3.2 eV, and around 2.4 to 2.8 eV for tungsten oxide (TAHIR *et al.* 2017), so sodium tungstate as precursor can produce material with modified physical characteristics. Literature usually reports only tungsten oxide formation under the same experimental conditions. One of the objectives of this work is to characterize the mix of products obtained when tungsten oxide is used as precursor.

On the other hand, the search for nanostructured tungsten oxide has led to much research using structuring agents, which affects the final morphology. Usually, non-ionic surfactants, such as polyethylene glycol (PEG) (TAHIR *et al.*, 2017), Triton X (WANG; PANG; HODGSON, 2009) and anionic surfactants, such as sodium dodecylsulphate (SDS) (KHARADE *et al.*, 2011; PAZINATO *et al.*, 2019) and stearic acid (PAZINATO; GARCIA, 2022) were used for coordination with tungsten atoms. The use of cationic surfactants is not very common, because the interaction is not with tungsten, but with oxygen bonded to tungsten, so there are few reports. However, two reports describe the use of cetyltrimethylammonium bromide (CTAB) as a shape-directing agent (GHOSH *et al.*, 2014).

We studied the influence of the cationic surfactant dodecyltrimetylammonium chloride (DTAC) as structuring agent of tungstate anions (and polyanions) in aqueous media. Films obtained from these systems were characterized with respect to their morphology, crystal structure and photocatalytic properties.

Materials and Methods

The precursor system was composed of sodium tungstate dihydrate, $Na_2WO_4.2H_2O$ (99.0% purity,

Fmaia™), hydrochloric acid (36.5–38.0%, Synth™) and the structuring agent dodecyltrimethylammonium chloride, DTAC, (99.0% purity, FlukaTM). The solutions were prepared with distilled water purified by a Milli-Q system (Millipore Inc.). The substrate was silicon (100), p-type, 50 ím thickness purchased from Chris Baker Co. Commercial WO_3 (99.0% purity, Aldrich™) was used for Raman analysis comparison. Hydrogen peroxide (29.0%, Synth™) and methyl orange (MO) dye (99%, Merck™) were used in the photocatalytic tests.

Film preparation and structural characterization

Silicon [100] coated with a 50 nm silicon oxide layer was used as substrate (SiO_2/Si). Prior to the film preparation, the substrates were immersed in concentrated sulfuric acid (10% v/v) for 15 min, and subsequently rinsed with distilled water and dried at 120 °C for 30 min.

Precursor systems containing 20 mmol·L^{-1} sodium tungstate dihydrate were studied in the presence of the structuring agent in concentrations which ranged from 0 to 100 mmol·L^{-1} DTAC. To prepare the systems, stock aqueous solution containing 100 mmol·L^{-1} DTAC were diluted to the final DTAC concentration with 20 mmol·L^{-1} $Na_2WO_4.2H_2O$.

The conversion of the tungstate/surfactant to tungstic acid/surfactant was performed by adjusting the pH to 1–2 by adding hydrochloric acid (95%), at 25 °C.

Tungstic acid/surfactant systems were spin coated onto SiO_2/silicon substrates (1000 rpm, 45 s). The films were dried at 110 °C for 1 h, and subsequently calcined at 700 °C for 3 h in a ceramic tube chamber, at atmospheric pressure in air. The calcination in air aims to remove the surfactant and water from the films.

In order to guarantee that all sodium tungstate were converted in tungstic acid, the films obtained as above were immersed in acid medium (pH~3) for 48 h and recalcined at 700 °C for 3 h at atmospheric pressure in air.

The scanning electron microscopy (SEM) was performed on the surface and cross-section of the films. SEM and energy dispersive x-ray spectroscopy (EDS) in an Evo Carl Zeiss microscope at 15kV. Films were coated with a 15-20 nm carbon layer. The average particle diameters were obtained with Image J™ software.

The Raman spectra were obtained with a Horiba Jobin Yvon spectrometer by the incidence of a He-Ne 10 mW laser at wavelength 632.9 nm.

X-ray Diffraction (XRD) was performed in a Siemens D500 diffractometer with Cu $K_<$ radiation (|_= 0.1542 nm). The diffraction spectra were registered at 2θ , between 10 and 60°, step 0.05°.

Photocatalytic performance

The photocatalytic performance of the tungsten oxide films was evaluated through the degradation of methyl orange dye (MO) in aqueous solutions containing hydrogen peroxide as initiator.

First it is necessary to optimize dye and hydrogen peroxide concentrations, because high concentrations of hydrogen peroxide overlay the action of the photocatalyst; otherwise, at high MO concentrations, the absorption of the radiation by the dye prevents the photons from reaching the film surface, which results in undervaluation of the photocatalyst efficiency. The optimal concentrations were determined as 1.05×10^{-3} mmol·L^{-1} hydrogen peroxide and 4.5×10^{-2} mmol·L^{-1} MO dye.

The photodegradation reactions were carried out in a quartz cell with 15 mL of dye solution. On the back internal face of the cell there is a support for a thin film. Films of area 6.25 cm^2 were fixed vertically against the anterior face of the cell, and a UVC vertical Philips 11 W lamp was placed 10 cm distant from the front face of the cell. The light intensity was evaluated by iron oxalate chemical actinometry and was 5.6×10^{-9} einstein. s^{-1}. The distance between the film and the front face of the cell was 2 cm (the distance from the light source to the film surface was 12 cm). Films, in contact with the dye solution, were left in the dark for the first 10 min to determine the decrease in concentration promoted by adsorption.

The MO concentration was evaluated by UV-vis photometry, monitoring the absorbance at 464 nm of the aliquots taken from the dye solution, as a function of time. To compare with the degradation promoted only by hydrogen peroxide, degradation tests also were conducted without films, by exposure of the dye/initiator system to radiation.

Results and Discussion

Film characterization

The cross-sectional views, exemplified in Fig.1-a, permitted determination of the thickness of the films, which ranged between 850 and 650 ⎡m, and decreased with the increase in DTAC concentration.

Figure 1 - (a) Cross section micrograph of the film obtained from aqueous systems containing 20 mmol·L^{-1} $Na_2WO_4 \cdot 2H_2O$ and 2.5 mmol·L^{-1} DTAC; micrographs (50000x magnification) of the film obtained from aqueous systems containing 20 mmol·L^{-1} $Na_2WO_4 \cdot 2H_2O$ with: (b) 2.5; (c) 10, (d) 20 and (e) 40 mmol·L^{-1} DTAC. Inset: particle size distribution. f) EDS of the film obtained from the systems containing 20.0 mmol·L^{-1} $Na_2WO_4.2H_2O$ with 10.0 40.0 mmol·L^{-1} DTAC. Inset: region of higher energy.

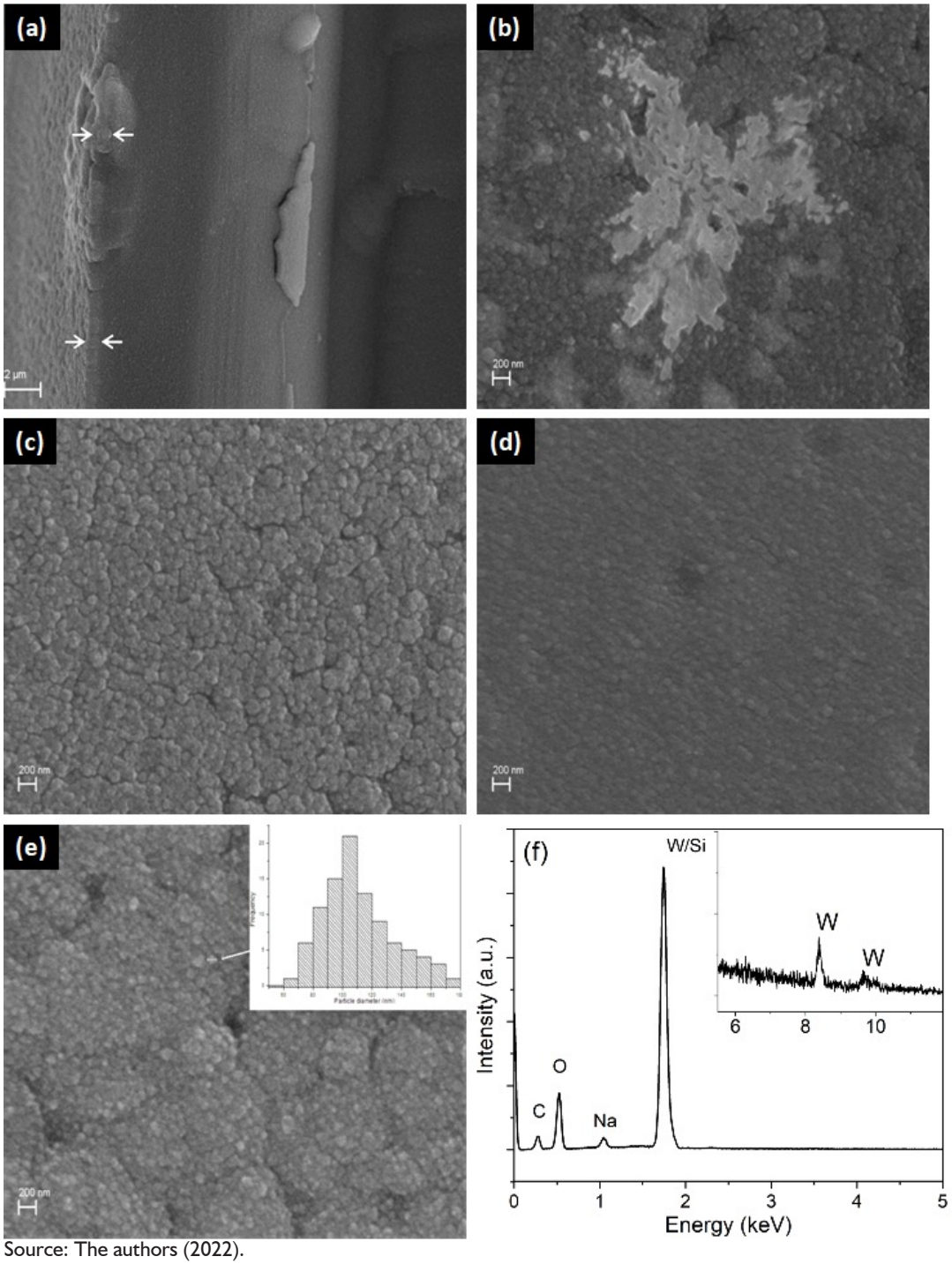

Source: The authors (2022).

The micrographs, Fig. 1-b, 1-c, 1-d and 1-e show the surface of the films obtained with 20 mmol·L^{-1} $Na_2WO_4 \cdot 2H_2O$ and in 2.5, 10, 20 and 40 mmol·L^{-1} DTAC, respectively. Films produced with low DTAC concentrations were very irregular (Fig. 1-b). The low surfactant concentration is responsible for the growth of precipitates during the removal of water.

The irregularity of the film morphology (Fig. 1-b) did not permit us to measure the particle diameter. Films with regular structures composed of nanospheres were obtained from aqueous systems in DTAC concentrations closer to the critical micellar concentration, 20 mmol·L^{-1} DTAC (Figs. 1-c, 1-d and 1-e). The average particle diameters are displayed in the bottom of the images and show that the surfactant plays an important role in structuring the precursor.

The observed decrease in particle size can be attributed to the interaction between the cationic part of the surfactant with the oxygen atoms of the tungstic acid and polytungstic clusters, formed in aqueous media, which resulted, after calcination, in a regular distribution of the tungsten species on the substrate surface.

Energy dispersive spectrum of the films surface (Fig. 1-f) reveals the presence of sodium (seen at 1.1 keV), tungsten, oxygen (0.5 keV) and carbon (0.25 keV). Carbon originates from the conductive coating used for SEM analysis. The signals of the tungsten, as well as the silicon substrate, are situated at 1.76 keV. Tungsten is confirmed through the peaks at 8.37 and 9.63 keV. Sodium, present in the calcined films, is attributed to sodium polytungstates; it will be discussed further.

Raman spectra of the films, shown in insert Fig. 2-a, are shifted vertically. The bands situated at 138 and 188 cm^{-1} are lattice vibrations WANG; PANG; HODGSON, 2009). Peaks A and B are bending vibrations of O–W(VI)–O bonds. Bands D, E and F are due to the stretching vibrations of O–W(VI)–O and can be originated of the tungsten oxide with large crystals. Sodium tetratungstate, $Na_2W_4O_{13}$ crystals are revealed by the C and E bands (KHARADE *et al*., 2011). The stretching vibrations of O–W linkages, contained in edge-shared WO_6 octahedra for this compound appear at 777–782 cm^{-1}(GHOSH *et al*., 2014). The presence of sodium ditungstate (832 cm^{-1}) or remaining sodium tungstate (311, 811 and 927 cm^{-1}) was not observed. The sharp peaks situated at 945 cm^{-1} do not permit discrimination between W=O from terminal tungsten oxide crystals and W-O- bonds (WU *et al*., 2013) (a bond between tungsten and unshared oxygen atoms is expressed as W-O- anion due to sodium tetratungstate) (KHARADE *et al*., 2011; GHOSH *et al*., 2014).

The presence of triclinic sodium tetratungstate and monoclinic tungsten trioxide films are also corroborated by XRD spectra (Figs. 2-c). Their presence was observed for films obtained at all ranges of DTAC concentrations studied.

The bands at 520 cm^{-1}, attributed to the SiO_2/Si substrate, were not observed for films obtained with low DTAC concentration, but were observed for films produced at higher surfactant concentrations (Fig. 2-a). This observation is in agreement with the reduction of the thickness with increasing DTAC concentration.

Fig. 2-b shows the Raman signal of the films´ surface after the test for removal sodium polytungstates (films were immersed in acid medium (pH~3) for 48 h and recalcined at 700 °C for 3 h at atmospheric pressure in air) in comparison with the pristine films. The Raman spectrum of the film submitted to the second treatment show bands referring to tungsten oxide, however it's possible to see also that the band at 775 cm^{-1}, related to $Na_2W_4O_{13}$ still remains. Also, bands at 258 and 750 cm^{-1} can be related to sodium ditungstate ($Na_2W_2O_7$). The species $Na_2W_2O_7$ and $Na_2W_4O_{13}$ may have been formed through reaction between tungsten oxide and sodium tungstate, forming $Na_2W_2O_7$, as well as $Na_2W_4O_{13}$. This explains the presence of sodium observed by EDS.

Figure II - **a) Raman spectra of the films obtained from aqueous systems containing 20 mmol·L^{-1} $Na_2WO_4 \cdot 2H_2O$ with: 10 to 100 mmol·L^{-1} DTAC after calcining for 3 h at 700 °C. b) Raman spectra of the films from aqueous systems containing 20 mmol·L^{-1} $Na_2WO_4 \cdot 2H_2O$ with 10 mmol·L^{-1} DTAC; c) XRD of the calcined films obtained from the aqueous systems containing 20 mmol·L^{-1} $Na_2WO_4 \cdot 2H_2O$ with: (c) 10, 50 and 100 mmol·L^{-1} DTAC after calcining for 3 h at 700 °C and (d) 20 mmol·L^{-1} DTAC after calcining for 3h at 700 °C. (+) Triclinic $Na_2W_4O_{13}$ and (#) monoclinic WO_3.**

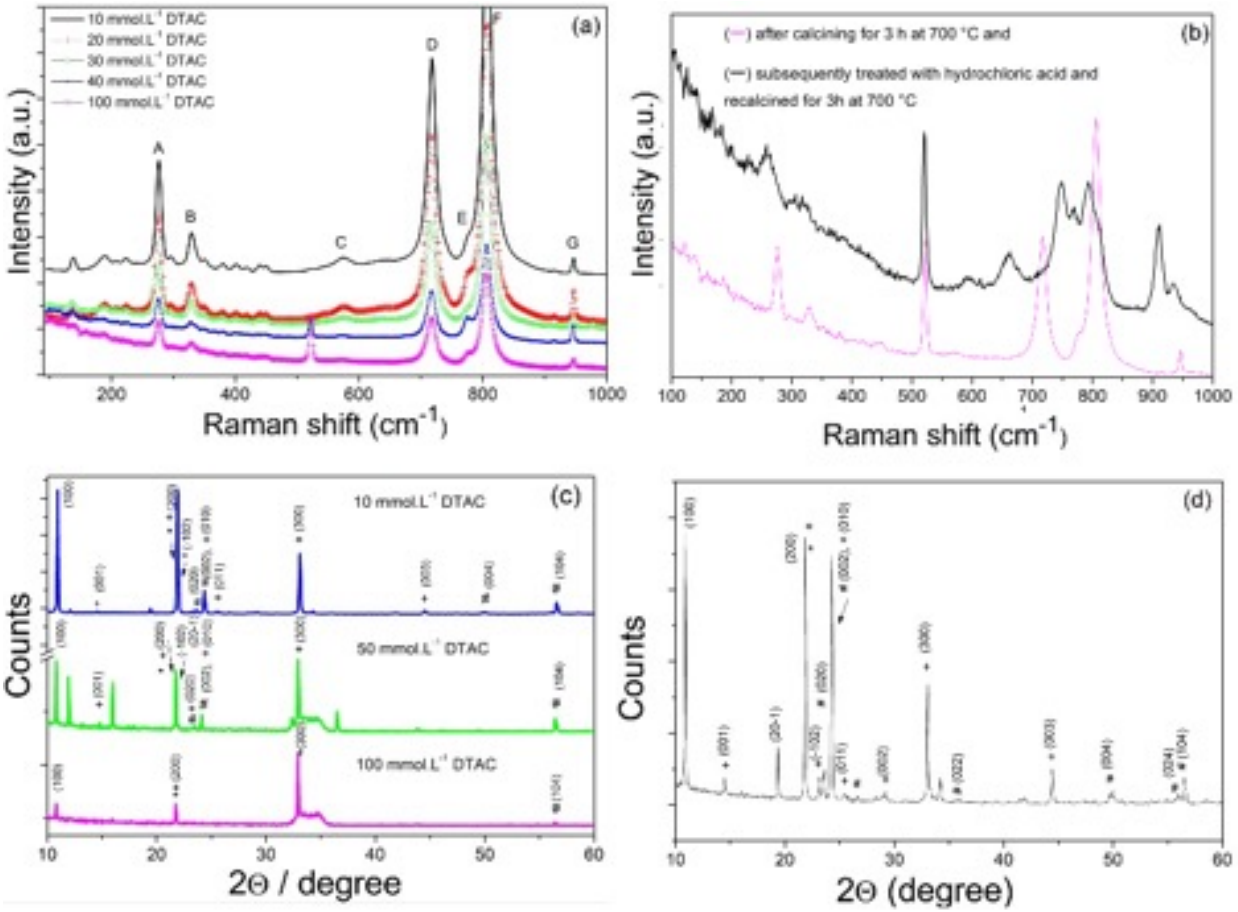

Source: The authors (2022).

The X-ray diffractograms, Fig. 2-c and 2-d, were analyzed with Match 3.0 softwareTM and permitted characterization of the films as triclinic $Na_2W_4O_{13}$, space group P-1 (PDF 70-2022) as the major phase, and monoclinic tungsten oxide, WO_3, space group P 1 21/c 1, (ISCD 647640) as the secondary phase (Fig. 2-c). DTAC concentration did not significantly affect the crystal structure or the stoichiometry of the films. Films obtained with a solution of 10 and 100 mmol·L^{-1} DTAC were composed of triclinic sodium tetratungstate and tungsten trioxide.

The polytungstate anions is not usually reported for sol-gel in aqueous medium processes, but we infer that the addition of acid to the sodium tungstate solution up to pH 1–2 also contributes to polytungstates structuring. This result can be explained by the hydrolysis of the tungstate with formation of polytungstate and hydroxyl ions [48] and agrees with previous study by Freedman, which reported the formation of poly anions through the reaction:

$$n\,WO_4^{-2} + (n+1)\,H_2O \rightarrow [H_{(n-1)}(WO_4)_n.2H_2O]^{-(n+1)} + (n-1)OH^- \qquad (I)$$

In presence of polyanions, the sol-gel process results in, after calcination, not only tungsten oxide, as usually reported, but a mixture of tungsten oxide and polytungstates

Photocatalytic performance

The optimal hydrogen peroxide concentrations, found by monitoring MO degradation as a function of time is 1.05×10^{-3} mmol·L^{-1} H_2O_2, which is not so high. At this concentration, peroxide acts only as initiator

of the photocatalytic process and was used in the photocatalytic test.

The results obtained by degradation of MO in presence of the synthesized films, are shown in Fig.3. The MO concentration as a function of time monitored for the system photocatalyst/MO/H2O2 in the dark shows that dye degradation is not significant and allow us to conclude that adsorption phenomena are not significant.

Figure III - MO concentration of 4.5 × 10^{-2} mmol·L^{-1} MO/1.05 × 10^{-3} mmol·L^{-1} H_2O_2 solutions in dark and under UVC (100-280 nm) radiation at 25 °C: with and without film synthesized from precursor system containing 20 mmol·L^{-1} DTAC.

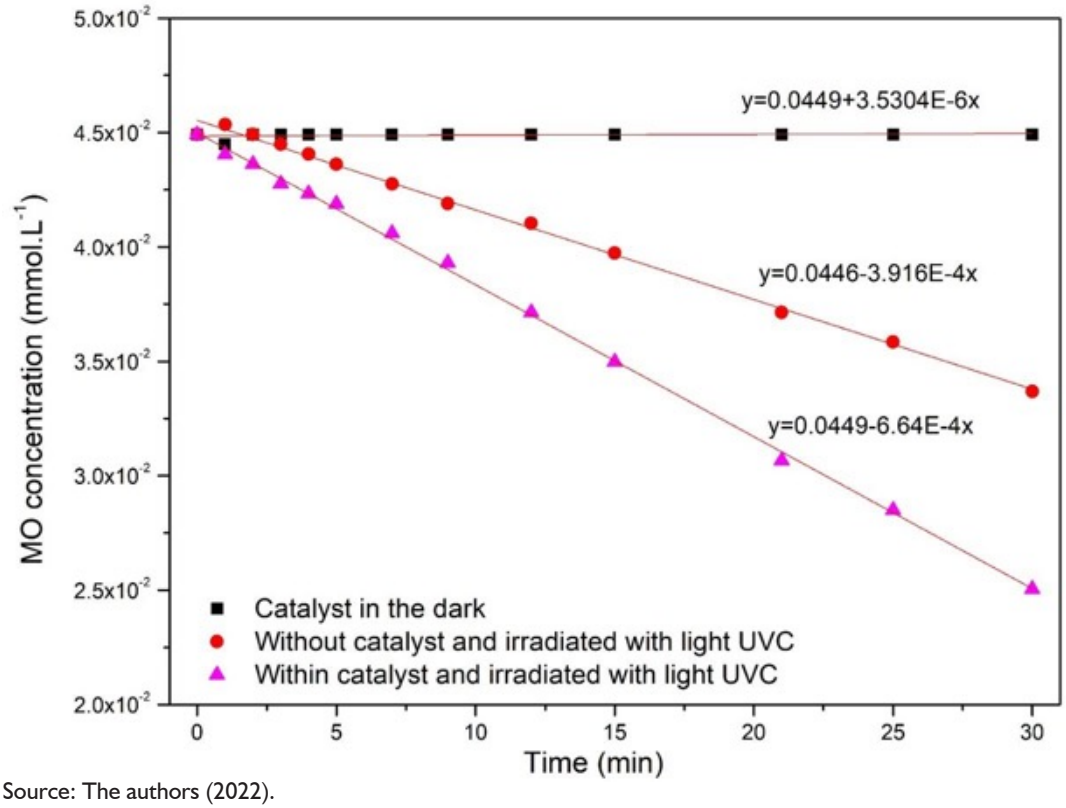

Source: The authors (2022).

The degradation reaction of MO follows a zero-order kinetics. After irradiated during 30 min, the MO/H_2O_2 system (without the photocatalyst) showed 35% of dye degraded. After a similar period, the degradations of the dye irradiated in the presence of the films, obtained from the precursor systems with 20 mmol·L^{-1} DTAC, was 41.0%.

The rate coefficients at 25 °C were 3.92x10^{-4} and 6.64x10^{-4} mmol·L^{-1}·min^{-1} for the non-catalyzed system and photocatalyzed system, respectively. The increase in rate coefficient, even observed, optimized and can be explained by the characteristics of sodium tetratungstate, which is a wide band gap material. The synthesized material presents also, sodium tetratungstate, which needs to be minimized in the obtention of photocatalytic materials. Pure tungsten oxide presents better performance to degrade MO dye (DA COSTA, 2015; GARCIA, 2015). It is important to report that the films did not lixiviate after photocatalysis experiment.

Conclusions

Films composed of triclinic sodium tetratungstate and monoclinic tungsten oxide were obtained from precursor system containing 20 mmol·L^{-1}sodium tungstate, at DTAC concentrations up to 100 mmol·L^{-1}, after reaction with hydrochloric acid, subsequent deposition on SiO_2/Si substrate and heat treatment at 700 °C for 3 h, in the presence of air.

DTAC concentration affected films morphology, producing irregular aggregates, in lower critical micellar concentrations, and regular films, structured as nanospheres, in higher concentrations. This behavior led us to infer that the ammonium cation of the surfactant interacts with the oxygen of tungstate and polytungstate anions, promoting regular distribution on the film surface.

The crystal structure was not significantly influenced by DTAC concentration, and was composed mainly of triclinic sodium tetratungstate and monoclinic tungsten oxide. The rate constant increased in presence of the photocatalyst synthesized from 20 mmol·L^{-1} sodium tungstate and 20 mmol·L^{-1} DTAC aqueous systems. The presence of sodium tetratungstate, which is a wide band gap material (~3.2 eV) is a probable reason for this behavior. To minimize sodium tetratungstate is important to prepare a material which has the potential to be engaged in the conversion of solar energy into chemical energy.

Acknowledgements

Authors thank to Coordenação de Aperfeiçoamento de Pessoal de Nível Superior (0001) and Fundação de Amparo à pesquisa do Estado do RS (FAPERGS), Proc. 21/2551-0002178-0, for the financial support.

References

CORRÊA, D. S.; PAZINATO, J. C. O.; FREITAS, M. A.; DORNELES, L. S.; RADTKE, C.; GARCIA, I. T. S.Tungsten oxide thin films grown by thermal evaporation with high resistance to leaching.**Journal of the Brazilian Chemical Society,** v. 26, p. 822-830, 2014. DOI: https://doi.org/10.5935/0103-5053.20140041. Disponível em: DOI: 10.5935/0103-5053.20140041 (crossref.org). Acesso em: 27 jan. 2022.

DA COSTA, N. B. D., PAZINATO, J. C. O.; SOMBRIO, G.; PEREIRA, M. B.; BOUDINOV, H.; GUNDEL, A.; MOREIRA, E. C.; GARCIA, I. T. S. Tungsten oxide thin films obtained by anodisation in low electrolyte concentration.**Thin Solid Films,** v. 578, p. 124-132, 2015. DOI: https://doi.org/10.1016/j.tsf.2015.02.031. Disponível em: https://www.sciencedirect.com/science/article/abs/pii/S0040609015001492?via%3Dihub. Acesso em: 20 jan. 2022.

DA COSTA, N. B. D.; PAZINATO, J. C. O.; SOMBRIO, G.; PEREIRA, M. B.; BOUDINOV, H.; GÜNDEL, A.; MOREIRA, E. C.; GARCIA, I. T. S. Controlling the structural and optical properties of tungsten oxide films synthesized under environmentally friendly conditions. **Materials Science in Semiconductor Processing,** v. 122, p. 105476, 2021. DOI: https://doi.org/10.1016/j.mssp.2020.105476. Disponível em: https://www.sciencedirect.com/science/article/abs/pii/S1369800120314104?via%3Dihub Acesso em: 17 jan. 2022.

DE MOURA, D. S.; PAZINATO, J. C. O.; PEREIRA, M. B.; MERTINS, O.; SILVA, E. M.; GARCIA, I. T. S. Poly(vinyl alcohol) as a structuring agent for peroxotungstic acid. **Journal of Molecular Liquids,** v. 269, p. 92-100, 2018. DOI: https://doi.org/10.1016/j.molliq.2018.08.015. Disponível em: Poly(vinyl alcohol) as a structuring agent for peroxotungstic acid - ScienceDirect. Acesso em: 20 fev. 2022.

FREEDMAN, M. L. Polymerization of anions – the hydrolysis of sodium tungstate and sodium chromate, **J. Am. Chem. Soc.** V. 80, p. 2072-2077, 1958.

GARCIA, I.T.S.; CORRÊA, D.S.; DE MOURA, D.S.; PAZINATO, J.C.O.; PEREIRA, M.B.; DA COSTA, N.B.D. Multifaceted tungsten oxide films grown by thermal evaporation. **Surface and Coatings Technology,** v.283, p. 177-183, 2015. DOI: https://doi.org/10.1016/j.surfcoat.2015.10.053. Acesso em: 27 fev. 2022.

GHOSH, S.; ACHARYYA, S.S.; TIWARI, R.; SARKAR, B.; SINGHA, R.K.; PENDEM, C.; SASAKI, T.; BAL, R. Selective Oxidation of Propylene to Propylene Oxide over Silver-Supported Tungsten Oxide Nanostructure with Molecular Oxygen.**ACS Catalysis,** v. 4, p. 2169-2174, 2014.DOI: https://doi.org/10.1021/cs5004454. Disponível em: Selective Oxidation of Propylene to Propylene Oxide over Silver-Supported Tungsten Oxide Nanostructure with Molecular Oxygen | ACS Catalysis. Acesso em: 27 mai 2022.

GURCUOGLU, O.; EVECAN, D.; ZAYIM, E.O. Synthesis and characterization of tungsten oxide films by electrodeposition with various precursors and electrochromic device application. **Journal of Solid State Electrochemistry,** v. 19, p. 403-413, 2015. DOI: https://doi.org/10.1007/s10008-014-2605-x. Disponível

em: Synthesis and characterization of tungsten oxide films by electrodeposition with various precursors and electrochromic device application | SpringerLink. Acesso em: 27 mai 2022.

KHARADE, R.R.; PATIL, S.P.; MANE, R.M.; PATIL, P.S.; BHOSALE, P.N. Synthesis and electrochromic application of surfactants tailored WO3 nanostructures. **Optical Materials**, v. 34, p. 322-326, 2011. DOI: https://doi.org/10.1016/j.optmat.2011.09.005. Disponível em: https://www.sciencedirect.com/science/article/abs/pii/S092534671100450 2?via%3Dihub. Acesso em: 20 mai 2022.

KUMAR, K. N.; SHAIK, H.; GUPTA, J.; SATTAR, S. A.; JAFRI R. I.; PAWAR, A.; MADHAVI, V.; REDDY, A.; NITHYA, G. Sputter deposited tungsten oxide thin films and nanopillars: Electrochromic perspective. **Materials Chemistry and Physics,** v. 278, p. 125706, 2022.DOI: https://doi.org/10.1016/j.matchemphys.2022.125706. Disponível em: https://www.sciencedirect.com/science/article/abs/pii/S0254058422000128. Acesso em: 20 jun 2022.

MARINHO, J. Z.; PATROCINIO, A. O. T. Nanomaterials and Their Thin Films for Photocatalytic Air Purification. In: Sabu Thomas; Merin Sara Thomas; Laly A Pothen. (Org.). **Nanotechnology for Environmental Remediation.** 12ed. Weinheim, Germany: Wiley Online Library, 2022, p. 341-359 DOI: https://doi.org/10.1002/9783527834143.ch18. Acesso em 09 set. 2022.

NAVIO, C.; VALLEJOS, S.; STOYCHEVA, T.; LLOBET, E.; CORREIG, X.; SNYDERS, R.; BLACKMAN, C.; UMEK, P.; KE, X.X.; VAN TENDELOO, G.; BITTENCOURT, C. Gold clusters on WO3 nanoneedles grown via AACVD: XPS and TEM studies. **Materials Chemistry and Physics,** v. 134, p. 809-813, 2012. DOI: https://doi.org/10.1016/j.matchemphys.2012.03.073. Disponível em: Gold clusters on WO3 nanoneedles grown via AACVD: XPS and TEM studies - ScienceDirect. Acesso em: 27 mai 2022 Acesso em: 27 mai 2022.

PAZINATO, J. C. O.; Marcos A. VILLETTI, M.A; MERTINS, O.; SILVA, E. R.; GARCIA, I. T. S. Insights on Structuration of Peroxotungstic Acid in Aqueous Media. **J. Braz. Chem. Soc.**, V. 30, P. 752-763, 2019. DOI: http://dx.doi.org/10.21577/0103-5053.20180196. Disponível em: 2018-0455AR.pdf (sbq.org.br). Acesso em: 9 set 2022.

PAZINATO, J. C. O.; GARCIA, I. T. S. Sub-stoichiometric tungsten oxide by the stearic acid method. **Ceramics International,** v. 48, p. 11971-11980, 2022. DOI: https://doi.org/10.1016/j.ceramint.2022.01.046. Disponível em: Sub-stoichiometric tungsten oxide by the stearic acid method - ScienceDirect. Acesso em: 27 mai 2022.

PICQUART, M.; CASTRO-GARCIA, S.; LIVAGE, J.; JULIEN, C.; HARO-PONIATOWSKI, E. Structural studies during gelation of WO3 investigated by in-situ Raman spectroscopy. **Journal of Sol-Gel Science and Technology,** v. 18, p. 199-206, 2000. DOI: https://doi.org/10.1023/A:1008775318802. Disponível em: Structural Studies During Gelation of WO3 Investigated by In-situ Raman Spectroscopy | SpringerLink. Acesso em: 10 jan. 2022.

PURUSHOTHAMEN, K.K.; MURALIDHARAN, G.; VIJAYAKUMAR, S. Sol-Gel coated WO3 thin films based complementary electrochromic smart Windows. **Materials Letters,** v. 296, p. 129881, 2021. DOI: https://doi.org/10.1016/j.matlet.2021.129881. Disponível em: Sol-Gel coated WO3 thin films based complementary electrochromic smart windows - ScienceDirect. Acesso em: 10 jan. 2022.

SANTATO, C.; ODZIEMKOWSKI, M.; ULMANN, M.; AUGUSTYNSKI, J. Crystallographically oriented Mesoporous WO3 films: Synthesis, characterization, and applications. **Journal of the American Chemical Society,** v. 123, p. 10639-10649, 2001. DOI: https://doi.org/10.1021/ja011315x. Disponível em: Crystallographically Oriented Mesoporous WO3 Films: Synthesis, Characterization, and Applications | Journal of the American Chemical Society (acs.org). Acesso em: 10 jan. 2022.

SCHOFIELD, K. A new method to minimize high-temperature corrosion resulting from alkali sulfate and chloride deposition in combustion systems. I. Tungsten salts.**Energy Fuels,** v. 17, p. 191-203, 2003. DOI: https://doi.org/10.1021/ef0201681. Disponível em: A New Method to Minimize High-Temperature Corrosion Resulting from Alkali Sulfate and Chloride Deposition in Combustion Systems. I. Tungsten Salts | Energy & Fuels (acs.org). Acesso em: 10 jan. 2022.

SHAMAILA, S.; SAJJAD, A.K.L.; CHEN, F.; ZHANG, J.L. WO3/BiOCl, a novel heterojunction as visible light photocatalyst. **Journal of Colloid and Interface Science,** v. 356, p. 465-472, 2011.DOI: https://doi.org/10.1016/j.jcis.2011.01.015. Disponível em: WO3/BiOCl, a novel heterojunction as visible light photocatalyst - ScienceDirect. Acesso em: 10 jan. 2022.

TAHIR, M. B.; NABI, G.; RAFIQUE, M.; KHALID, N. R. Nanostructured-based WO3 photocatalysts: recent development, activity enhancement, perspectives and applications for wastewater treatment. **International Journal of Environmental Science and Technology,** v. 14, p. 2519-2542, 2017. DOI https://doi.org/10.1007/s13762-017-1394-z. Disponível em: Nanostructured-based WO3 photocatalysts: recent development, activity enhancement, perspectives and applications for wastewater treatment | SpringerLink. Acesso em: 10 set. 2022.

VAMVASAKIS, I.; GEORGAKI, I.; VERNARDOU, D.; KENANAKIS, G.; KATSARAKIS, N. Synthesis of WO3 catalytic powders: evaluation of photocatalytic activity under NUV/visible light irradiation and alkaline reaction pH. **Journal of Sol-Gel Science and Technology,** v.76, p. 120-128, 2015. DOI: https://doi.org/10.1007/s10971-015-3758-5. Disponível em: Synthesis of WO3 catalytic powders: evaluation of photocatalytic activity under NUV/visible light irradiation and alkaline reaction pH | SpringerLink. Acesso em: 10 jan. 2022.

WANG, S.H.; CHOU, T.C.; LIU, C.C. Nano-crystalline tungsten oxide NO2 sensor. **Sensors & Actuators, B: Chemical,** v. 94, p. 343-351, 2003. DOI: https://doi.org/10.1016/S0925-4005(03)00383-6. Disponível em: Nano-crystalline tungsten oxide NO2 sensor - ScienceDirect. Acesso em: 10 jan. 2022.

WANG, W.; PANG, Y.X.; HODGSON, S.N.B. XRD studies of thermally stable mesoporous tungsten oxide synthesised by a templated sol-gel process from tungstic acid precursor. **Microporous and Mesoporous Materials,** v. 121, p. 121-128, 2009. DOI: https://doi.org/10.1016/j.micromeso.2009.01.014. Disponível em: XRD studies of thermally stable mesoporous tungsten oxide synthesised by a templated sol–gel process from tungstic acid precursor - ScienceDirect. Acesso em: 10 jan. 2022.

WU, C.L.; WANG, C.K.; LIN, C.K.; WANG, S.C.; HUANG, J.L. Electrochromic properties of nanostructured tungsten oxide films prepared by surfactant-assisted sol-gel process. **Surface and Coatings Technology,** v. 231, p. 403-407, 2013. DOI: https://doi.org/10.1016/j.surfcoat.2012.01.061 Disponível em: https://www.sciencedirect.com/science/article/abs/pii/S025789721200771?via%3Dihub. Acesso em: 10 jan. 2022.

YANG, J.; LI, W.Z.; LI, J.; SUN, D.B.; CHEN, Q.Y. Hydrothermal synthesis and photoelectrochemical properties of vertically aligned tungsten trioxide (hydrate) plate-like arrays fabricated directly on FTO substrates. **Journal of Materials Chemistry,** v. 22, p. 17744-17752, 2012. DOI: https://doi.org/10.1039/C2JM33199C Disponível em: https://pubs.rsc.org/en/content/articlelanding/2012/jm/c2jm33199c. Acesso em: 10 jan. 2022.

ZHANG, Q.; WANG, R.; LU, Y.; WU, Y.; YUAN, J.; LIU, J. Highly Efficient Photochromic Tungsten Oxide@PNIPAM Composite Spheres with a Fast Response. **ACS Applied Materials & Interfaces,** v. 13, p.4220-4229, 2021. DOI: https://doi.org/10.1021/acsami.0c20817. Disponível em: Highly Efficient Photochromic Tungsten Oxide@PNIPAM Composite Spheres with a Fast Response | ACS Applied Materials & Interfaces. Acesso em: 19 jan. 2022.